Impedance probe to measure local gas volume fraction and bubble velocity in a bubbly liquid

R. Zenit, D. L. Koch, and A. S. Sangani

Citation: Rev. Sci. Instrum. **74**, 2817 (2003); doi: 10.1063/1.1569391

View online: http://dx.doi.org/10.1063/1.1569391

View Table of Contents: http://rsi.aip.org/resource/1/RSINAK/v74/i5

Published by the American Institute of Physics.

Impedance probe to measure local gas volume fraction and bubble velocity in a bubbly liquid

R. Zenit[a)]
Instituto de Investigaciones en Materiales, Universidad Nacional Autónoma de México, Apartado, Postal 70-360, Ciudad Universitaria, Coyoacán, México D.F. 04510, México

D. L. Koch
School of Chemical Engineering, Cornell University, Ithaca, New York 14853

A. S. Sangani
Department of Chemical Engineering and Materials Science, Syracuse University, Syracuse, New York 13244

(Received 17 December 2001; accepted 2 March 2003)

We have developed a dual impedance-based probe that can simultaneously measure the bubble velocity and the gas volume fraction in length scales comparable to the bubble diameter. The accurate determination of the profiles is very important for comparisons with existing theories that describe the rheological behavior of bubbly liquids. The gas volume fraction is determined by the residence time of bubble within the measuring volume of the probe. We have found that the details of the bubble-probe interactions must be taken into account to obtain an accurate measure of the gas volume fraction at a point. We are able to predict the apparent nonlinear behavior of the gas volume fraction measurement at large concentrations. The bubble velocity is obtained from the cross correlation of the signals of two closely spaced identical probes. Performance tests and results are shown for bubble velocity and bubble concentration profiles in a gravity driven shear flow of a bubbly liquid. © *2003 American Institute of Physics.* [DOI: 10.1063/1.1569391]

I. INTRODUCTION

Recently, there have been significant advances in the theory of inertial suspensions, in particular those that describe the rheology of bubble suspensions. For the case of a bubble suspension in which the Reynolds number is large and the Weber number is small, a complete set of governing equations can be composed from first principles.[1,2] The extent of the validity of these theories could only be assessed if comparisons with detailed experimental measurements are performed. Hence, there is a need for accurate measurements of velocity and concentration profiles.

Impedance techniques are widely used in the multiphase flows community to obtain measurements of volume fractions.[3] In most cases such techniques are limited to obtain a spatial average of the volume fraction since the volume through which the measurement is performed is much larger than the individual bubble size. Techniques that can obtain a point-wise measurement of the gas volume fraction are less common.[4–6] The technique presented here is a modification of that designed by Waniewski,[4] who used an impedance probe to measure the gas volume fraction profiles caused by the air entrained by a plunging bow wave. To obtain a local measurement of the gas volume fraction, the measuring volume associated with the probe has to be small enough to detect individual bubbles. This characteristic of the measuring system is essential to measure the spatial variations of the bubble concentration. To obtain accurate measurements it is particularly important, as it will be explained later, to account for the bubble–probe interaction for the case when the bubbles are deflected rather than pierced by the measuring probe. The system implemented by Liu and Bankoff[5] was also used to obtain point-wise measurements of the gas volume fraction in a bubbly column. In their case, the size of the probes was much smaller than the typical bubble size. Liu and Bankoff argued that the bubbles were pierced during their interaction with the probe but provided no further information to justify this claim. Also, no details were given about the electronics used or the frequency response of their system. Cartellier[6] was able to obtain simultaneous measurements of the local void and bubble velocity using a single optical probe. In this case, the bubbles were also pierced by the probe but careful experiments were performed to describe the interaction between the bubbles and the probe during this process.

There exist several other techniques to measure volume fraction in a multiphase flow which include light attenuation,[7] transmission of gamma rays,[8] neutron radiography,[9] etc. All of these techniques are limited to obtain line or volume average measurements.

In addition to the measurement of the gas volume fraction, the presented system is capable of measuring the bubble velocity by cross correlating the signals of two identical probes placed at a small distance. Measurements of the bubble velocity and bubble velocity variance can be obtained with a high degree of accuracy. Detailed sets of experimental results and their comparisons with theoretical predictions can be found in Refs. 10 and 11.

a)Electronic mail: zenit@servidor.unam.mx

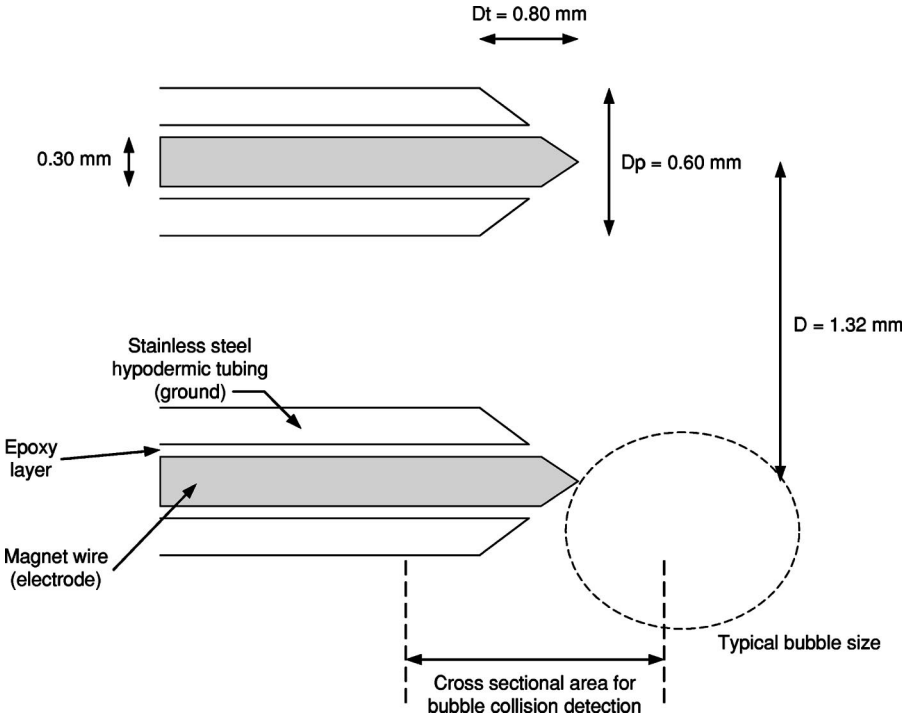

FIG. 1. Sketch of the dual impedance probe.

II. DESIGN

The system detects local changes of electrical impedance in a bubbly liquid. It uses the difference in electrical impedance between the gas and liquid phases to determine the residence time of bubbles in a small measuring volume adjacent to the probe tip. The probe arrangement is shown schematically in Fig. 1 and the electronics that are used for the measurements are shown schematically in Fig. 2. An electrode is embedded in a thin hypodermic needle, which acts as the ground. The electrode carries a rapidly oscillating voltage (500 kHz). When bubbles pass near the tip of this probe, the local impedance and the current through the electrode are affected. The amplitude of the current signal is then converted to a dc voltage signal by a precision rectifier, which is filtered twice and amplified. The probes and electronic circuits used here are based on the system used in Ref. 4. The neddles used to fabricate the probes were 15 cm long with 0.63 and 0.33 mm of outer and inner diameters, respectively. The cable length from the probes to the data acquisition system was of 1.8 m. The resulting capacitance per unit of length of the probe cable array ranged from 1 to 4 nF/m.

A typical signal change detecting an individual bubble as it passes near the tip of the probe is shown in Fig. 3. The range of electric field around the tip of the probe is approximately 0.3 mm for the chosen value threshold level (inferred from the collision area measurements shown in Fig. 9).

A. Tests

The performance of the probe was tested in a tall vertical channel, shown in Fig. 4. The cell was fabricated with Plexiglass and had a thickness of 2 cm and a width of 20 cm. The cell was tall enough, 200 cm, for the velocity and voidage profiles to fully develop. Nitrogen gas was introduced at the base of the water filled channel through an array of capillaries that generated bubbles of approximately 1 mm in diameter, which satisfy the dual limit of small Weber number and large Reynolds number. A small amount of an electrolyte ($0.05\ \mathrm{mol\,L^{-1}}\ MgSO_4$) was added to the water to inhibit bubble–bubble coalescence. The addition of this small amount of salt does not change the viscosity or density of the liquid or the surface tension of the gas–liquid interface significantly. Figure 5 shows photographs of the bubbles produced for two typical mean gas concentrations.

To produce a nearly monodispersed bubble population

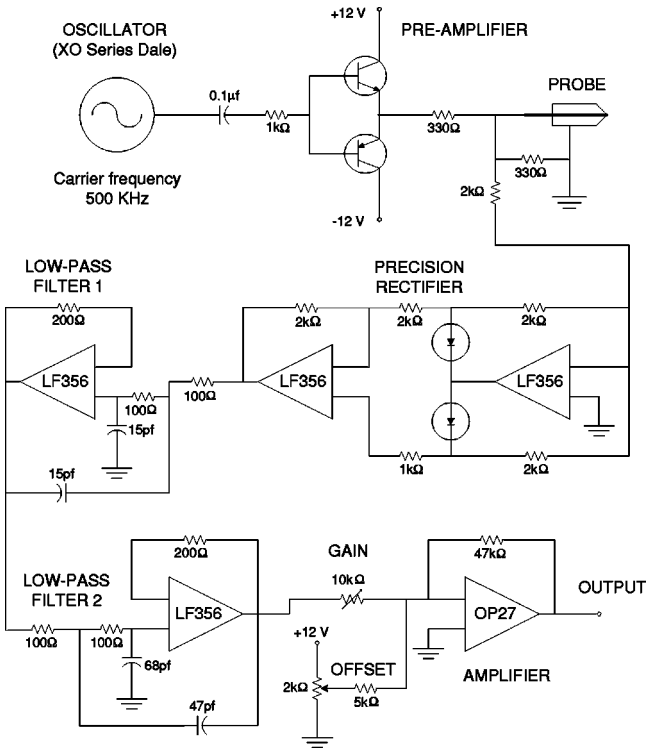

FIG. 2. Electronics schematic diagram.

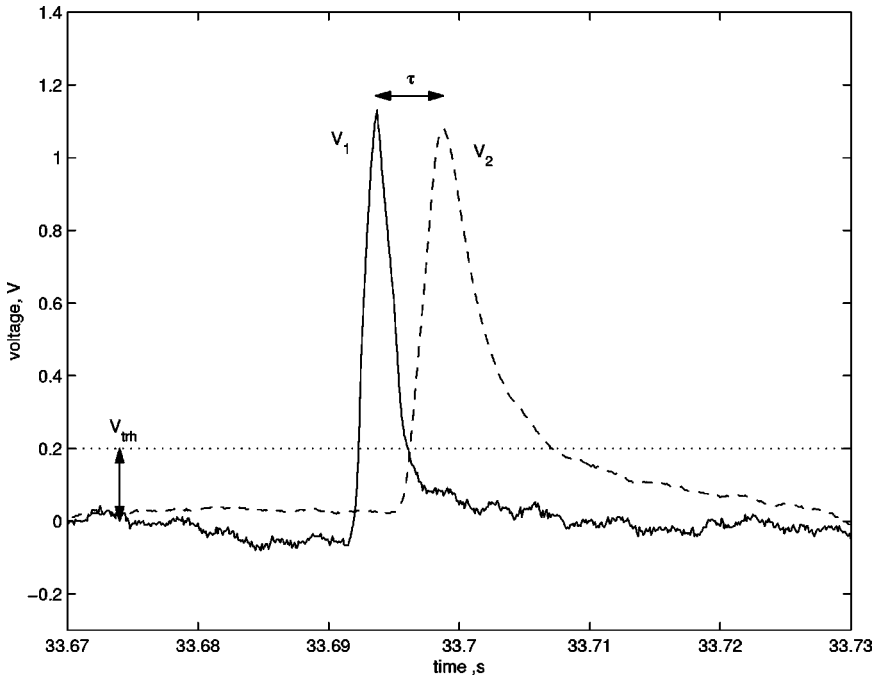

FIG. 3. Typical voltage signal resulting from a bubble passing near the tip of the probe. The solid line denotes the signal obtained from the leading probe, the dashed line shows the signal from the trailing probe. The dotted line denotes the voltage threshold level. The voltage threshold and the time delay between signals are also shown.

special attention had to be given to the design of the capillary array. The bank of capillaries had approximately 900 glass tubes. Each capillary was 65 mm long with an inner diameter of 100 μm. To achieve the maximum number of capillaries per unit of area, the tubes were positioned in a plate in a hexagonal array (28 capillaries per square cm). The gas flow through each capillary was small enough to ensure that the formation of a bubble at its tip was in a quasisteady fashion. The capillary bank was mounted at the bottom of the channel, between the cell and the Nitrogen chamber. More details on the construction of the array and the experimental setup can be found in Ref. 10.

The vertical channel provides a convenient setting in which the volume fraction measurement technique can be validated since the average bubble concentration, or gas volume fraction, can be inferred directly from the column hold up,

$$\alpha=(H_o/\Delta H+1)^{-1}, \tag{2.1}$$

where H_o is the initial liquid level, and ΔH is the liquid level

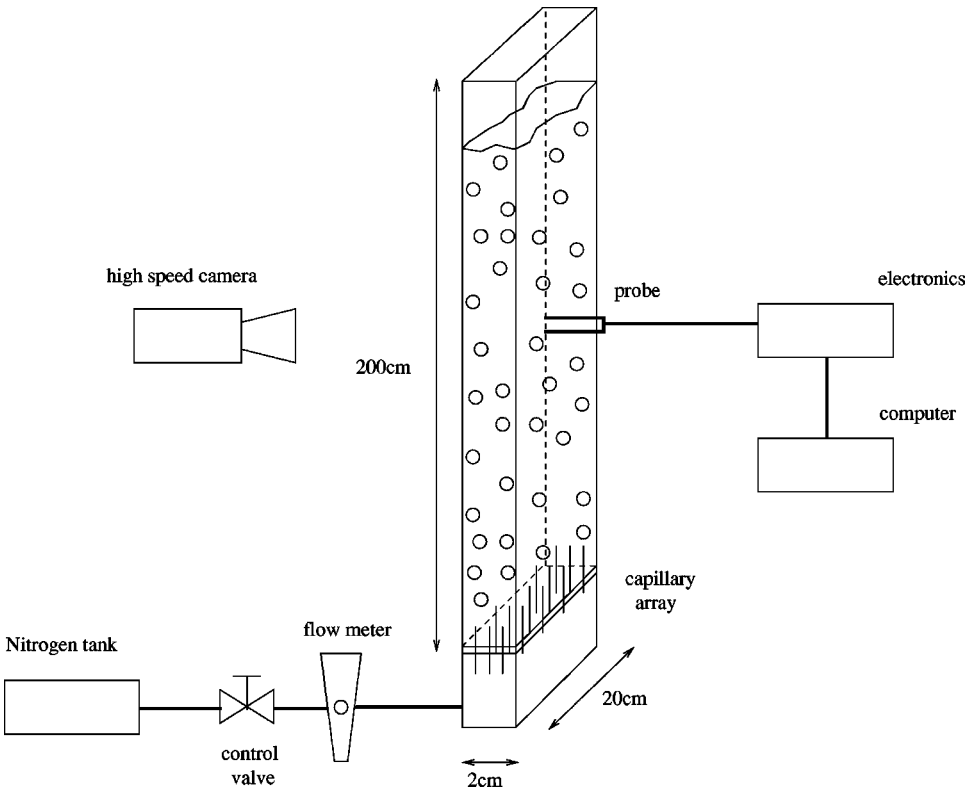

FIG. 4. Experimental setup.

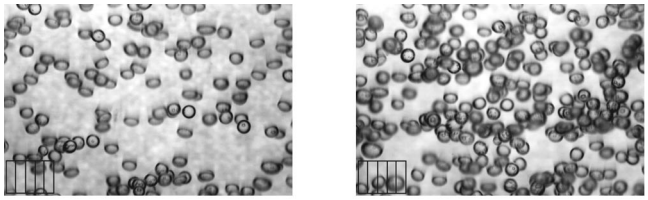

FIG. 5. Photographs of the flow for two typical gas volume fractions. The bubble size is nearly monodispersed for both cases. The spacing in the grid, shown in the lower-left corner, is 1 mm. (a) $\alpha=0.02$, (b) $\alpha=0.05$.

increase after the bubbles are introduced to the cell. Moreover, the increase of the gas volume fraction that results from the bubble motion through a hydrostatic pressure gradient is small (less than 4% for present conditions). Therefore, the measurement of the gas volume fraction obtained from the column hold up can be considered nearly uniform across the length of the channel. The interactions of the bubble with the containing walls can also produce gradients of the gas volume fraction near the walls. However, it has been demonstrated that these gradients do not extend much further than a few bubble diameters from the wall.[10]

Additionally, individual bubble tests had to be conducted to quantify the details of the bubble–probe interaction. These details are very important to properly measure the gas volume fraction for the conditions considered in this article. The tests were obtained in a $10\times10\times10$ cm^3 lucite container in which the probe could be mounted to one of its sides. The container was filled with the same electrolyte solution as the flow cell. Different capillaries could be introduced and positioned through the base of the container such that bubbles of different sizes and at different positions could interact with the dual impedance probe. A high-speed video camera was used to record the interaction of the bubbles with the probe. Using digital image processing techniques, the size, shape, and velocity of the bubble was determined.

III. GAS VOLUME FRACTION MEASUREMENTS

The basic measurement principle relies on the fact that it is possible to discriminate between the two phases by their difference in electric impedance. In order to quantify the phase fraction of each component, we need an electronic device capable of measuring the electric impedance in a nearly instantaneous manner.

If the period of the voltage oscillation, produced by the electronic device, is much shorter than the residence time of the bubble in the measuring volume, then the measurement can be considered to be instantaneous. The measuring volume is defined as the volume around the probe for which a bubble, whose centroid is within that volume, produces a signal $V>V_{\mathrm{trh}}$, where V_{trh} is a predetermined threshold level. Therefore, the duration of the pulse can be interpreted as the residence time of the bubble in the measuring volume. The residence time, and therefore, the apparent gas volume fraction, will depend on a predetermined discriminating threshold level. The local gas volume fraction is determined by the time average of the binary function $\beta(t)$ defined as,

$$\beta(t)=\begin{cases}1 & \text{if } V_1(t)>V_{\mathrm{trh}}\\ 0 & \text{if } V_1(t)\leqslant V_{\mathrm{trh}}\end{cases}, \tag{3.1}$$

where $V_1(t)$ is the voltage signal from the probe and V_{trh} is the threshold level. Therefore, the time-averaged gas volume fraction, β_m, is calculated from

$$\beta_m=\frac{1}{t_s}\int_0^{t_s}\beta(t)dt, \tag{3.2}$$

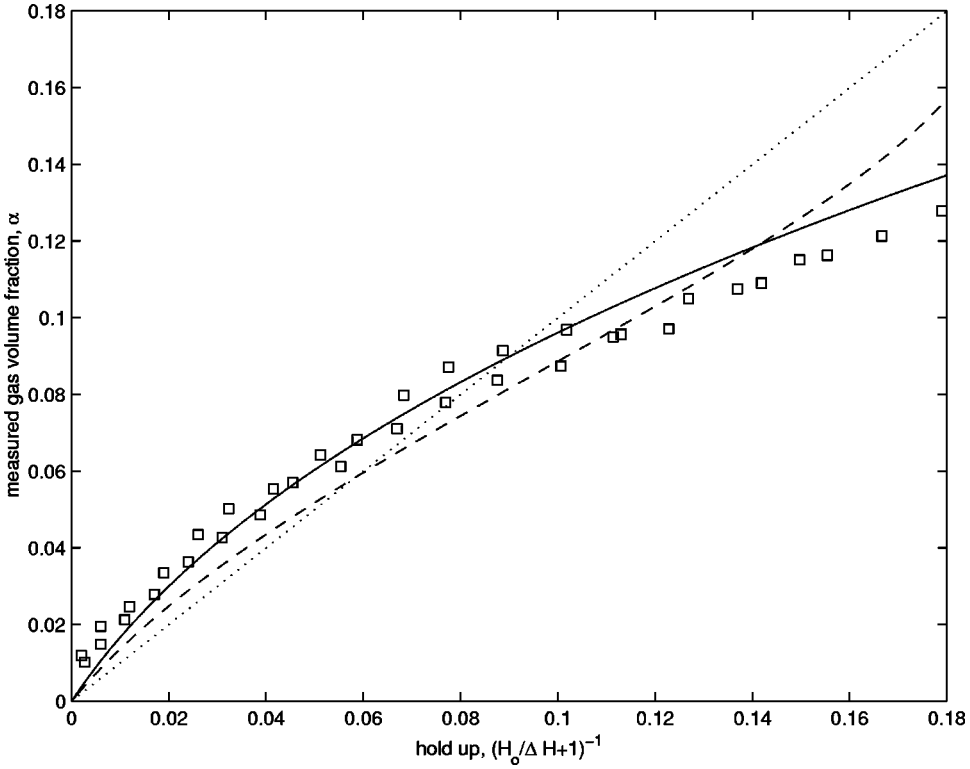

FIG. 6. Calibration of the impedance volume fraction probe. Comparison of the measured gas void fraction with the column hold up for a threshold level, $V_{\mathrm{trh}}=0.2$ V (□). The dotted line shows the correlation between the hold up and the fraction of time for which the signal is above the threshold value. The solid and dashed lines show the corrected hold up values considering the effect of the bubble–probe interaction [Eq. (3.3)]. The solid line considers constant bubble diameter and aspect ratio ($d_b=1.53$ mm, $\chi=1.19$); the dashed line shows the prediction considering the size and aspect ratio variations as a function of the hold up, from Ref. 10.

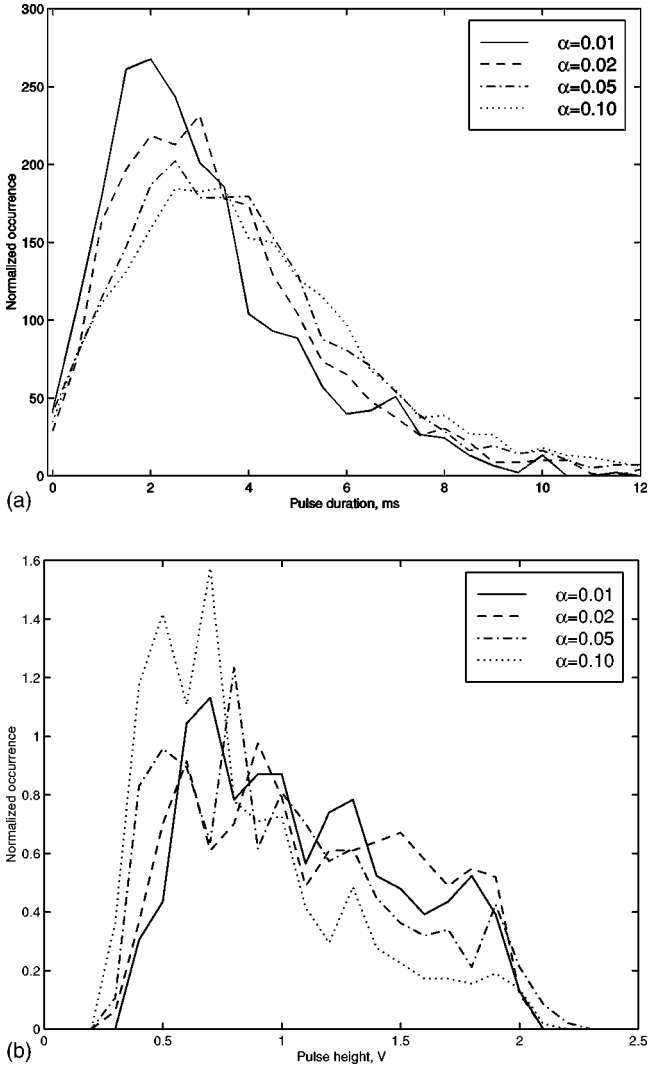

FIG. 7. Probability density function of the bubble detection pulse height and width for different gas volume fractions. The occurrence is normalized such that the integral under the curve is of value one. (a) Pulse width. (b) Pulse height.

where t_s is the total sampling time. The right-hand side of Eq. (3.2) can be alternatively interpreted as the product of the bubble number density and the measuring volume of the probe. Provided that the accessible measuring volume is equal to the bubble volume, the two methods of interpreting the signal measurement are the same. We have chosen a signal threshold level for which the measuring volume and bubble volume are approximately equal in the small gas volume fraction range ($\alpha < 0.01$).

The performance of the system is assessed by a calibration test. The probe is immersed in an environment in which the gas volume fraction is known. The measurement obtained from it, processing the signal using Eq. (3.2), is then compared with the known value of the gas volume fraction. In this manner the most appropriate threshold level is determined. The calibration test is shown in Fig. 6. The graph shows the measured gas volume fraction as a function of the mean column gas volume fraction. The column mean gas volume fraction, or hold up, is calculated using Eq. (2.1). The probe is positioned in the middle of the channel where the gas fraction is uniform; small variations occur only very close to the walls.[10] The value of β_m was calculated for a range of threshold values and it was found to increase for decreasing threshold levels, resulting from the increase of the measuring volume with the threshold level. A threshold voltage of 0.2 V was chosen such that the measured β_m approximates the holdup at small bubble volume fractions. The value of the threshold voltage is kept constant for all the subsequent tests to minimize the effect of this arbitrary choice. From Fig. 6, it can be noted that the measured gas volume fraction β_m shows an apparent nonlinear behavior as the value of the hold up increases. If the measurements were exact, the value of β_m and the hold up would be approximately the same and the measurements would follow the dotted line shown in Fig. 6. For the case shown, the measured volume fraction is slightly larger than the hold up for dilute cases, but as the concentration increases the value of β_m becomes smaller than the column hold up.

To further assess the performance of the probe the probability density functions of the time width and height of the bubble detections are calculated. These probability density functions are shown in Fig. 7 for different values of the mean gas volume fractions. The distribution of heights is similar for different gas volume fractions, which demonstrates that the system works in a similar fashion for different bubble concentration levels. On the other hand, the distribution of pulse widths changes as the concentration increases. Since the mean bubble velocity decreases with bubble concentrations, the collisions can be expected to have interactions of longer duration with the probe. The distribution of pulse width extends from nearly zero to 10 ms. The width of the duration distribution results from the fact that both the bubble size and bubble velocity have variations along a mean value. This width is also an indication that the bubbles are being retarded as a results of their interaction with the probe.

Although the bank of capillaries was designed to produce bubbles of a uniform size, a slight increase in size is observed as the bubble concentration increases.[10] Also, resulting from the increased hydrodynamic interactions, the bubbles become less oblate as the bubble concentration increases. Resulting from this increase of the bubble size, we can expect the accessible measuring volume for bubble detection to increase. It will be seen that this change in bubble diameter accounts for some of the nonlinear dependence of β_m on the holdup seen in Fig. 6. Impedance-based probes can be constructed to have a linear dependence of the measured gas volume fraction but, in general, the performance of such probes is based on spatial averages over many bubbles. In our case we are restricted to single bubble interactions to obtain point measurements.

A. Correction due to bubble–probe interaction

Clearly, the performance of the measuring system is not linear. We analyze the details of the bubble–probe interaction to find an explanation for the nonlinear response of the probe. The main difference of this measuring system with others previously used is the localized detection of individual bubbles. The system is designed to measure gas volume fraction at points. To achieve this goal the size of the measuring

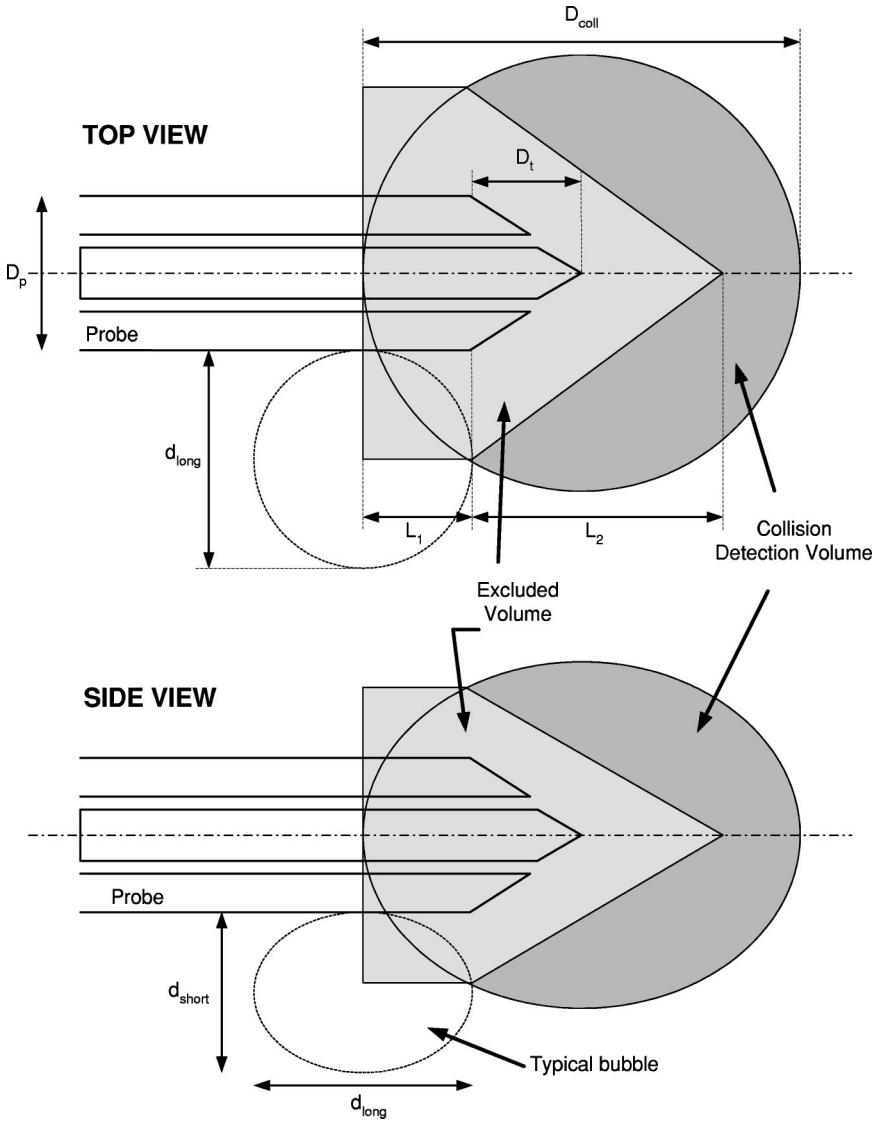

FIG. 8. Sketch of the geometry of the probe excluded volume and bubble collision detection volume.

volume had to be made small, of the same order as the bubble size. For this case, not all the bubbles are able to cross the measuring volume freely. Instead, a fraction of the bubbles that interact with the probe collide with it and are deflected. Hence, the measurement obtained from the probe, using Eq. (3.3), has to be corrected to obtain a more accurate value of the gas volume fraction.

Since some bubbles are deflected during the interaction with the probe and do not cross the bubble detection volume freely, we must account for a volume that is not accessible to all bubbles. We can define the accessible measuring volume as the difference between the collision detection volume and the excluded volume. We can reinterpret β_m as the time fraction at which bubbles are within the accessible measuring volume. The measured gas volume fraction can be written as

$$\beta_m = \frac{6\alpha}{\pi d_b^3}(V_{\text{coll}} - V_{\text{exc}}), \tag{3.3}$$

where β_m is the fraction of time for which the probe signal is above the threshold, α is the true gas volume fraction in the flow, and V_{coll} and V_{exc} are the collision detection and excluded volumes, respectively. A sketch of the excluded and detection volumes around the probe tip is shown in Fig. 8.

If we can find appropriate expressions for V_{coll} and V_{exc}, then a correction of the measured β_m can be obtained and, hence, the true gas volume fraction α can be calculated.

1. Collision detection volume

The collision detection volume is measured from a series of individual bubble experiments to determine the collision detection area. This area was quantified by analyzing the signal when single bubbles, released at different positions, interacted with the probe. Bubble collisions were identified when the resulting signal rose above the predetermined threshold. The collision area is the area at the tip of the probe within which bubble centers are detected. Tests were performed for different bubble sizes and for a range of bubble–probe distances. Figure 9 shows the measured collision area for three different bubble equivalent diameters. Clearly, the collision area increases with the bubble diameter. The relationship of the collision area with the bubble equivalent diameter d_{eq} can be fitted to the expression

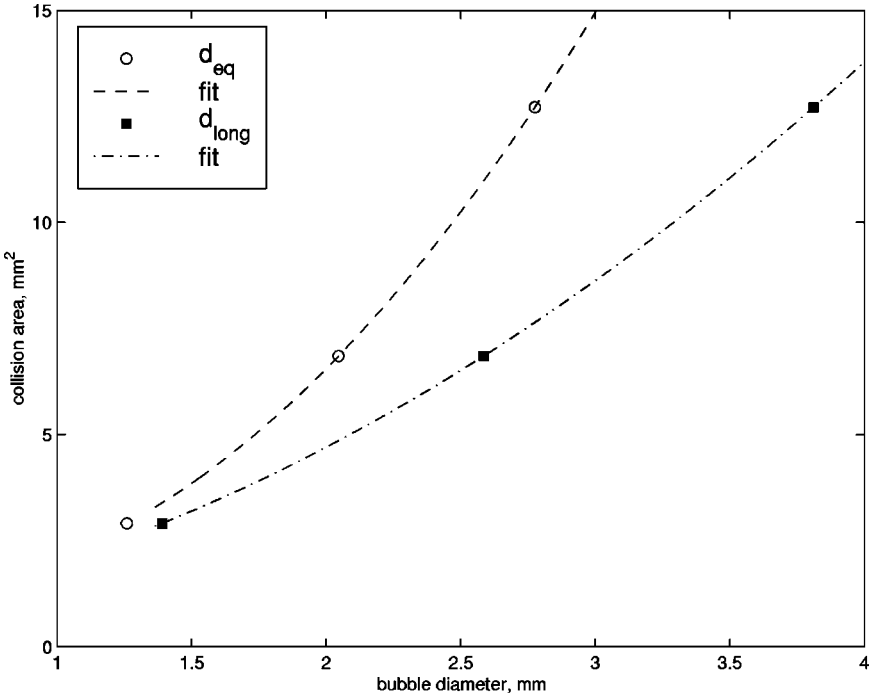

FIG. 9. Measured collision area as a function of the bubble equivalent diameter d_{eq} and bubble's long axis d_{long}. Lines show the fit to the measurements.

$$A_{\mathrm{coll}}=1.997d_{eq}^2-1.588d_{\mathrm{eq}}+1.747, \tag{3.4}$$

where $d_{\mathrm{eq}}=(d_{\mathrm{long}}^2 d_{\mathrm{short}})^{1/3}$, d_{long} and d_{short} are the long and short axes of the bubble, respectively. The equivalent bubble diameter and the collision detection area are given in mm and mm^2, respectively. This expression was obtained for a threshold level of 0.2 V. The collision detection volume is then inferred from the measured collision area by assuming the detection volume is an oblate spheroid, shown schematically in Fig. 8. The collision area is expected to be different for side-ways collisions because oblate bubbles have a shorter dimension in the vertical direction. Using the bubble aspect ratio, $\chi=d_{\mathrm{long}}/d_{\mathrm{short}}$, and the bubble equivalent diameter, d_{eq}, the collision volume can be written as

$$V_{\mathrm{coll}}=\frac{4}{3}\pi\left(\frac{D_{\mathrm{coll}}}{2}\right)^2\left(\frac{D_{\mathrm{coll}}}{2\chi}\right),$$

where $D_{\mathrm{coll}}=\sqrt{4A_{\mathrm{coll}}/\pi}$ is the diameter of the collision detection area. Therefore,

$$V_{\mathrm{coll}}=\frac{4}{3}\frac{A_{\mathrm{coll}}^{3/2}}{\sqrt{\pi}\chi}, \tag{3.5}$$

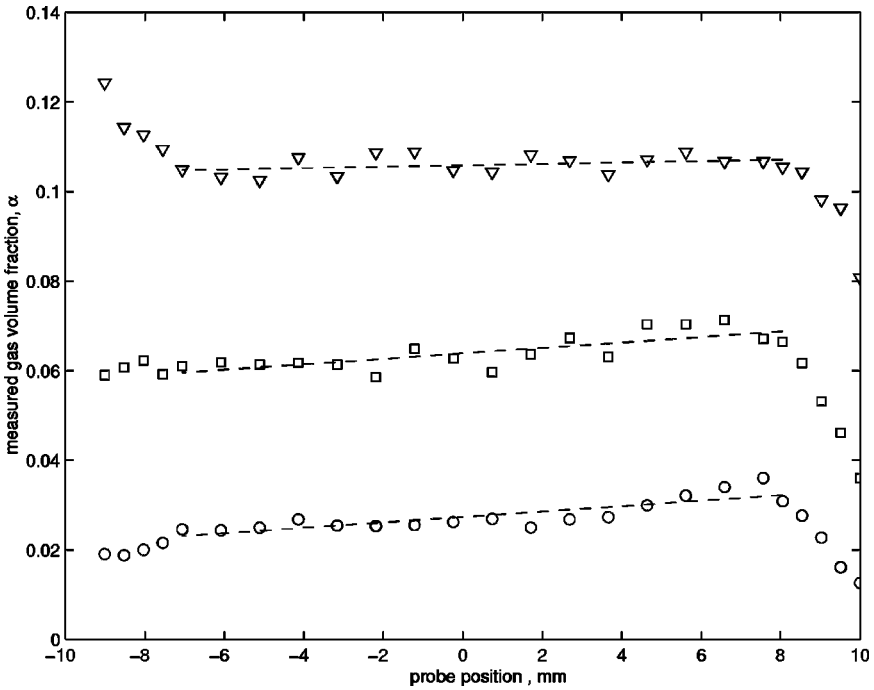

FIG. 10. Gas fraction profiles for three typical hold ups. (○), $\alpha=0.02$; (□), $\alpha=0.05$; and (∇), $\alpha=0.10$, for a channel inclination of $\theta=5°$. The lines show best linear fits of the data excluding the near-wall regions.

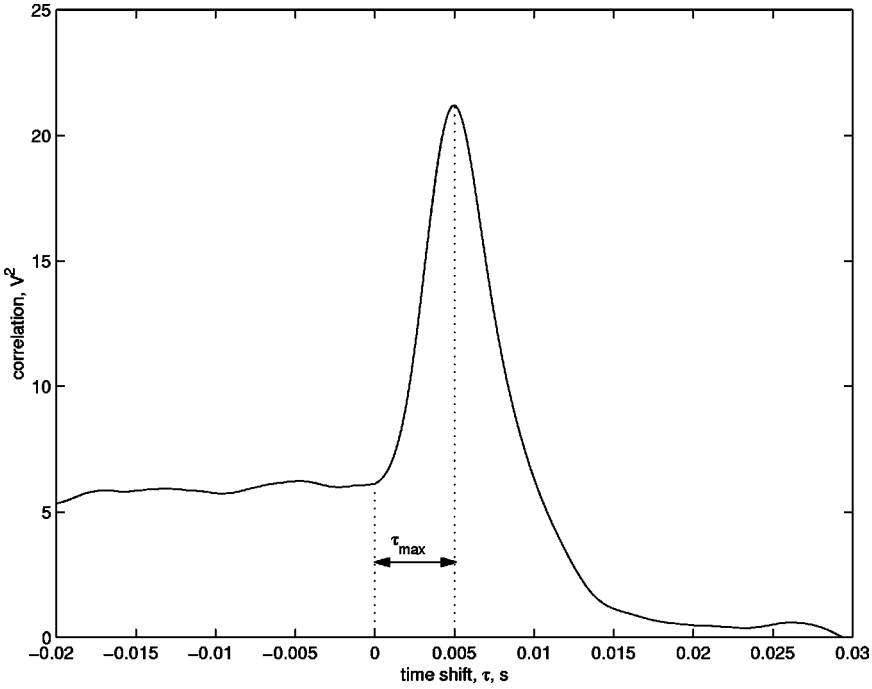

FIG. 11. Cross-correlation function as a function of the delay time. The line is that calculated from the signals shown in Fig. 3.

which is the volume of an oblate spheroid with the same aspect ratio as that of the bubbles.

2. Probe excluded volume

The centers of the bubbles that are sensed and counted to calculate the gas volume fraction must cross through the measuring volume of the probe. Due to the intrusive nature of the probe only part of the collision volume is accessible to bubble centers. Bubbles passing, for example, at the base of the probe will collide with the probe and be deflected; therefore, their residence time in the measuring volume will be reduced resulting in a reduction of the measured gas fraction. The excluded volume around the probe can be calculated assuming that it extends from the edge of the collision area to the tip of the probe and circumscribes a cross-sectional area proportional to the bubble diameter (as depicted in Fig. 8). The excluded volume can be expressed as

$$V_{\text{exc}} = V_{\text{prism}} + V_{\text{cone}} = L_1 A_{\text{base}} + \frac{L_2}{3} A_{\text{base}}$$

$$= A_{\text{base}} \left(L_1 + \frac{L_2}{3} \right),$$

where V_{prism} and V_{cone} are an ellipsoidal prism (that accounts for the base of the probe) and a cone (that accounts for the

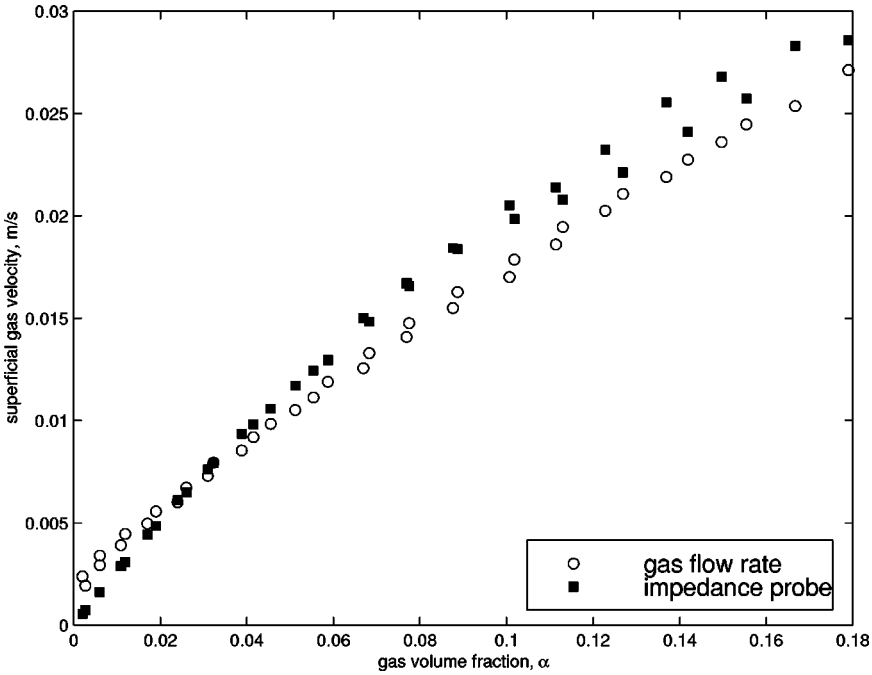

FIG. 12. Superficial gas velocity as a function of mean gas volume fraction. The size of the symbols denotes approximately the magnitude of the experimental error.

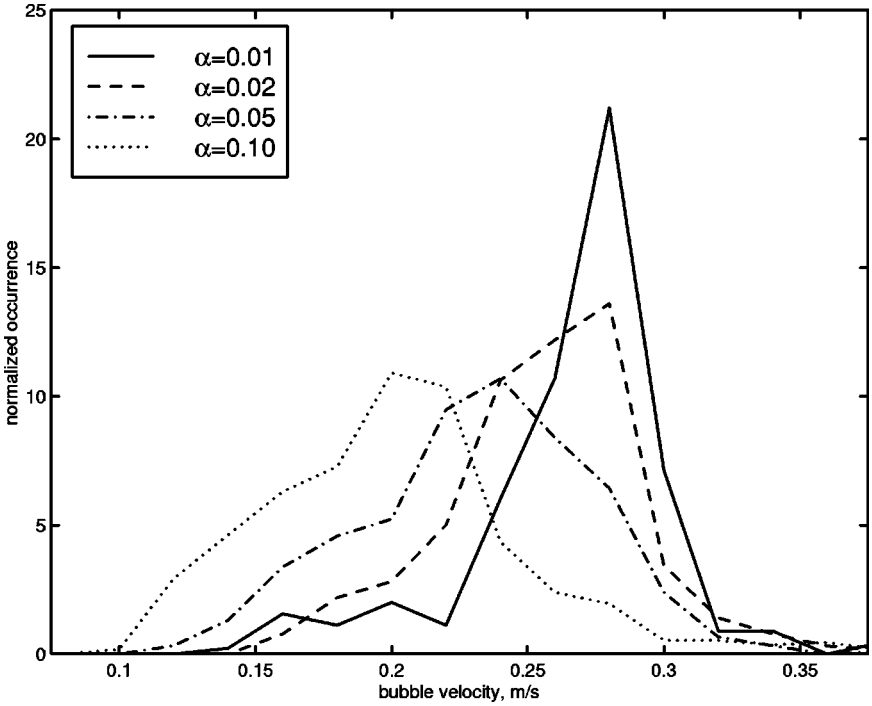

FIG. 13. Normalized bubble velocity probability density function for four typical gas volume fractions. The width of the bins is 0.02 m/s.

tip of the probe). L_1 is the length of the prism, which extends from the edge of the collision volume to the base of the probe tip:

$$L_1 = \sqrt{A_{\text{coll}}/\pi} - D_t,$$

and L_2 is the height of the cone, which includes the tip length, D_t, and a bubble radius:

$$L_2 = D_t + \frac{d_{\text{eq}}\chi^{1/3}}{2}.$$

The area of the base is an ellipse with the same aspect ratio as the bubbles:

$$A_{\text{base}} = \frac{\pi}{4}(D_p + d_{\text{eq}}\chi^{-2/3})(D_p + d_{\text{eq}}\chi^{1/3}),$$

where D_p is the diameter of the probe. These distances are depicted schematically on Fig. 8. We can now calculate the probe excluded volume as

$$V_{\text{exc}} = \left[\frac{\pi}{4}(D_p + d_{\text{eq}}\chi^{-2/3})(D_p + d_{\text{eq}}\chi^{1/3})\right]\left[(\sqrt{A_{\text{coll}}/\pi} - D_t) + \frac{1}{3}\left(D_t + \frac{d_{\text{eq}}\chi^{1/3}}{2}\right)\right]. \quad (3.6)$$

For the probe used in these experiments $D_p = 0.63$ mm and $D_t = 0.8$ mm. Clearly, the size of the excluded volume and the collision detection volume increase as the bubble diameter increases.

3. Corrected measurement

Since the equivalent bubble diameter and the bubble aspect ratio can be experimentally determined,[10] a correction for the excluded volume can be obtained to quantify the effect of the bubble–probe interaction on the measured value of the volume fraction. Figure 6 shows the prediction of Eq. (3.3) using the expressions for the V_{exc} and the V_{coll} shown above, considering constant (solid line) and changing (dashed line) bubble size and aspect ratio. Clearly, the correction captures the apparent nonlinear behavior of the sensor. Therefore, by applying this correction to the measurements obtained from the raw signal, a more accurate measurement of the gas volume fraction is obtained.

B. Example: Gas volume fraction profiles

The probe can be used to determine the spatial variations of the gas volume fraction in any flow. We show some typical results obtained for a gravity-driven shear flow of a bubbly liquid.[11] The calculations and the signal analysis are performed on the digitized voltages from the probe. The sampling rate used was 10 kHz. For each measurement a minimum of 100 s of signal was captured. The measured gas volume fraction as a function of probe position between the two walls is shown in Fig. 10, for different values of the mean gas volume fraction. Clearly, small changes of the gas volume fraction can be measured accurately using the probe. When the measuring point is near a wall the error involved in the measurement of the gas volume fraction increases due to the probe–wall interaction.

IV. BUBBLE VELOCITY MEASUREMENTS

A second identical probe can be positioned at a known distance above the leading probe. If a bubble passes near both probes, the signals produced in each of them will be similar but shifted in time, as shown in Fig. 3. The signals are cross-correlated and the delay time, $\tau_{\max}$, can be accurately calculated as the value of signal shift time τ that maximizes the cross-correlation function, $F_{V_1V_2}$, defined as

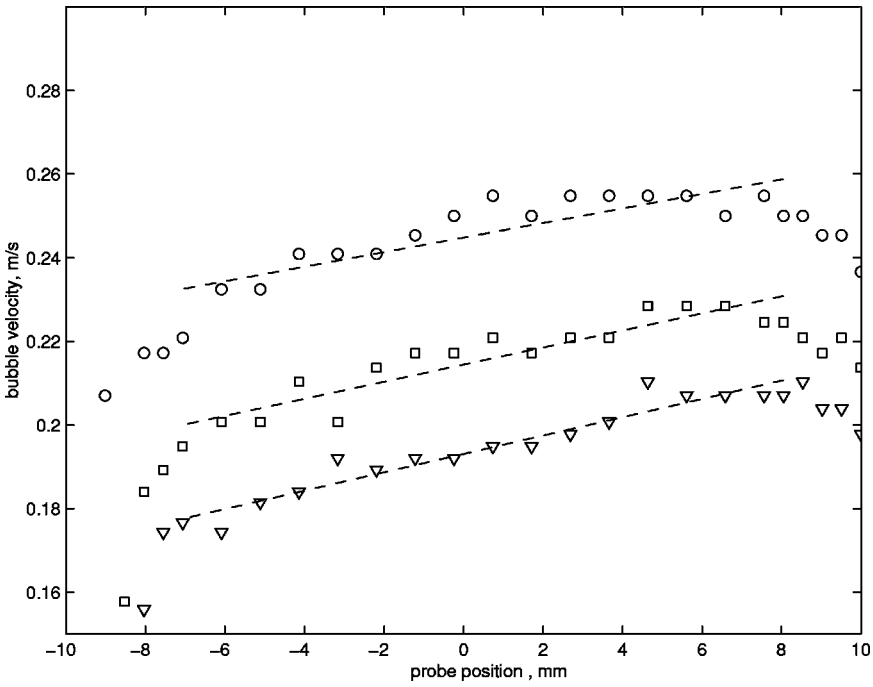

FIG. 14. Bubble velocity profiles for three typical hold ups. (○), $\alpha=0.02$; (□), $\alpha=0.05$; and (∇), $\alpha=0.10$, for a channel inclination of $\theta=5°$. The lines show the linear best fits.

$$F_{V_1V_2}(\tau)=\frac{1}{t_s}\int_0^{t_s} V_1(t)V_2(t-\tau)dt, \tag{4.1}$$

where t_s is the sampling time and V_1 and V_2 are the voltages obtained from the leading and trailing probes, respectively. Figure 11 shows the cross-correlation function $F_{V_1V_2}(\tau)$, obtained from the two signals shown in Fig. 3, as a function of the time shift τ. The plot shows a clear maximum value.

The bubble velocity is calculated by

$$u_b=\frac{D}{\tau_{\max}} \tag{4.2}$$

where D is the separation distance between probes. The separation between the probes is in accordance with the theoretical considerations of Ref. 12. The velocity calculated in this manner was compared with the velocity obtained using video image processing. The results differ only by 1% for a 1.3 mm bubble moving at 27 cm/s. Note that for this technique to be appropriate the bubble velocity must be nearly unidirectional, which is true for the flows considered here. The bubble velocity calculated from the cross-correlation function uses the entire time series (typically, 100 s) from the impedance probe. The resulting measurement contains information from many different bubble events.

To corroborate the accuracy of measured velocities a comparison can be performed between the superficial gas velocity $u_o=Q/A_o$ and the product of the holdup and the measured bubble velocity, $(u_b\alpha)$. Q is the volumetric gas flow rate and A_o is the cross-sectional area of the channel. Figure 12 shows a good comparison between the two quantities. At low concentration the superficial gas velocity measurements are slightly higher than the values measured directly with the impedance probe, but for more concentrated mixtures the measured bubble velocity is always larger than that calculated from the flow rate. It must be noted that the error in the measurement of the superficial gas velocity is on the order of 10%, which may explain the disagreement observed at larger concentrations.

Information concerning the probability distribution of bubble velocities can be obtained through further processing of the signals. The velocity of individual bubble can be obtained if similar pulse appear on the signals of both probes but shifted in time. If the time delay of this shift is calculated, a collection of individual bubble velocities can be obtained. Other important statistical measures, like the velocity variance, can be calculated. Since some of the bubbles that are sensed by the leading probe are deflected and, therefore, are not sensed by the trailing probe, a certain discriminating algorithm must be formulated to account for this effect. A program was written to search and identify voltage pulses corresponding to bubble detections by the leading probe, i.e., events for which the signal rises above the voltage threshold of 0.2 V. To determine if a similar pulse, shifted in time, was produced in the trailing probe, a *local* cross-correlation function is performed. A discriminating criterion is adopted to eliminate erroneous signals. If the calculated velocity is improbable, it is assumed that the signals in the two probes were caused by two different bubbles and, therefore, the trace is discarded. The algorithm discards velocities that are more than 50% larger than the terminal velocity and smaller than a tenth of the terminal velocity. In addition, events that yield small values of the maximum in the cross-correlation function, $F_{V_1V_2}<0.0015V^2$, are discarded. The sample length used for the determination of the local cross-correlation function is 20 ms. Figure 13 shows typical probability distribution functions for the bubble velocity at different gas volume fractions. The distribution of bubble velocities can be determined with the presented system.

A. Example: Bubble velocity profiles

As in the example shown for the gas volume fraction measurements, we show the bubble velocity profiles obtained in a gravity-driven shear flow.[11] The signals are acquired using the same parameters as those used for the gas volume fraction measurements. Bubble velocity profiles are shown in Fig. 14 for three different values of the mean gas volume fraction. Clearly, the velocity profiles can be determined with a good degree of accuracy. The velocity, in the cases shown, changes only by 12% along the width of the channel but the change is captured accurately with the dual probe.

V. DISCUSSION

The main difficulty in performing localized measurements in a bubbly flow arises from the bubble–probe interaction mechanism. Generally, small bubbles are not pierced by the probe during their interaction. Since bubbles are deflected as a result of the collision with the probe, the measured signal does not represent the true value of the gas volume fraction at that point. Accounting for the excluded volume produced by the probe itself, we are able to correct the raw measurement to obtain a higher degree of accuracy. With the proposed system the velocity and distribution of velocities of the bubbles are also obtained. The development and implementation of the presented system is relatively simple and low cost.

ACKNOWLEDGMENTS

This work was supported by NASA under Grant No. NAG3-1853 and by CONACyT Grant No. J34497U-2.

[1] S. A. Kang, A. S. Sangani, H.-K. Tsao, and D. L. Koch, Phys. Fluids **9**, 1540 (1997).
[2] P. D. M. Spelt and A. S. Sangani, Appl. Sci. Res. **58**, 337 (1998).
[3] S. L. Ceccio and D. L. Georges, J. Fluids Eng. **118**, 391 (1996).
[4] T. A. Waniewski, Ph.D. thesis, California Institute of Technology (1999).
[5] T. J. Liu and S. G. Bankoff, Int. J. Heat Mass Transf. **36**, 1061 (1993).
[6] A. Cartellier, Rev. Sci. Instrum. **63**, 5442 (1992).
[7] D. M. Leppinen and S. B. Dalziel, Exp. Fluids **30**, 214 (2001).
[8] H. V. Kok, T. H. J. J. van der Hagen, and R. F. Mudde, Int. J. Multiphase Flow **27**, 147 (2001).
[9] K. Mishima and T. Hibiki, Nucl. Eng. Des. **184**, 183 (1998).
[10] R. Zenit, D. L. Koch, and A. S. Sangani, J. Fluid Mech. **429**, 307 (2001).
[11] R. Zenit, Y. H. Tsang, D. L. Koch, and A. S. Sangani, *J. Fluid Mech.* (submitted).
[12] Q. Wu, K. Welter, D. McCreary, and J. N. Reyes, Flow Meas. Instrum. **12**, 43 (2001).